Passive fluidic diode for simple fluids using nested nanochannel structures

Jingwen Mo,[1] Long Li,[1] Jun Wang,[2] and Zhigang Li[1,*]

[1]*Department of Mechanical and Aerospace Engineering, The Hong Kong University of Science and Technology, Clear Water Bay, Kowloon, Hong Kong*

[2]*Key Laboratory of Enhanced Heat Transfer and Energy Conservation, Ministry of Education, College of Environmental and Energy Engineering, Beijing University of Technology, Beijing 100124, People's Republic of China*

(Received 17 December 2015; published 4 March 2016)

In this paper, we propose a moving part-free fluidic diode for simple fluids using nested nanochannels, which contain inner and outer channels of different lengths. Molecular dynamics simulations show that the fluidic diode accepts water flows in the forward direction and blocks flows in the backward direction in a wide range of pressure drops. The anisotropic flow rates are generated by the distinct activation pressures in different directions. In the forward direction, the activation pressure is low, which is determined by the infiltration pressure of the inner channel. In the backward direction, the activation pressure is quite high due to the capillary effects when flows are released from the inner to the outer channel. The pressure drop range for the fluidic diode can be varied by changing the channel size or surface wettability. The fluidic diode offers an alternative way for flow control in integrated micro- and nanofluidic devices.

DOI: 10.1103/PhysRevE.93.033101

I. INTRODUCTION

The invention of electronic diodes made it possible to easily control electric currents and played a critical role in the miniaturization of electronic circuits and devices [1,2]. Their exceptional rectification effects have motivated the exploration for the control of other flows, such as heat, fluid, and acoustic flows [3–10]. In fluidic systems, flow regulations through fluidic diodes can be easily realized by using certain moving parts, such as check valves [11–13]. However, as fluidic systems scale down to micro- or nanoscale, those moving parts may cause reliability issues and increase the fabrication cost. In small scale fluidic systems, passive fluidic diodes (no moving parts) are preferred for flow manipulations [14–18]. Unfortunately, fluid transport is different from electron transport, and it is quite challenging to achieve unidirectional flows through fixed structures for simple fluids. Although a nanofluidic diode has been fabricated recently [10], extensive work is required to develop diverse fluidic diodes to promote the applications of micro- and nanofluidic systems in various areas, including biology, medicine, chemistry, and engineering [19].

In fixed structures, it is difficult to completely block fluid flows in a direction. In contrast, it is relatively easier to design fluidic rectifiers, which allow fluid flows in both the forward and the backward directions but with different flow rates. In the literature, most efforts were focused on the development of fluidic rectifiers [20–24]. Conventional passive fluidic rectifiers employ asymmetric structures to generate direction dependent flow resistance where flow rectifications can only be achieved at high Reynolds numbers or by using non-Newtonian fluids [10,25]. Nonetheless, the performance of these rectifiers is rather poor. The diodicity, which is defined as the flow rate or pressure drop ratio between the forward and the backward directions, is usually less than 6 [10,25,26].

The development of fluidic diodes is in the early stage. Fortunately, progress has been made in the past few years. Some fluidic diodes have been reported through surface modifications [10,27,28]. A paper-based fluidic diode between an anode and a cathode was fabricated by depositing a surfactant on the anode through click chemistry, which allowed unidirectional flows from the anode to the cathode [27]. Another fluidic diode was realized by coating one side of a porous paper towel such that the surface energy is tuned to change the flow resistance [28]. Although unidirectional flows were achieved in these diodes, the flows were caused by wicking effects, and the performance of the diodes under relatively high pressures was unclear. In addition, these paper-based diodes were single-use devices and could not be integrated into complex fluidic systems. Recently, we fabricated a fluidic diode using nanochannels of heterogeneous surface energies where water flows were blocked in one direction for a range of pressure drops due to the potential energy barrier at the entrance on the hydrophobic side of the channels [10]. The potential energy barrier was caused by the van der Waals interactions between fluid molecules and channel atoms. The idea of taking advantage of molecular interactions on the nanoscale can lead to diverse designs for flow rectifications.

Herein, we propose a simple fluidic diode using nested nanochannels, which consist of two slit channels of different sizes with the smaller one embedded into the larger one. Molecular dynamics (MD) simulations show that water flowing from the small channel to the large channel (backward direction) is blocked in a wide range of pressure drops, which can be tuned by changing the surface wettability or channel height. The blockage in the backward direction is caused by the large pressure difference across the water meniscus as the water moves from the small channel to the large channel.

II. MOLECULAR DYNAMICS SIMULATIONS

The nested nanochannel structure contains two slit nanochannels of different heights and lengths between two reservoirs as illustrated in Fig. 1. The dimensions of the simulation cell in the y and z directions are 11.5 and 4.1 nm,

*mezli@ust.hk

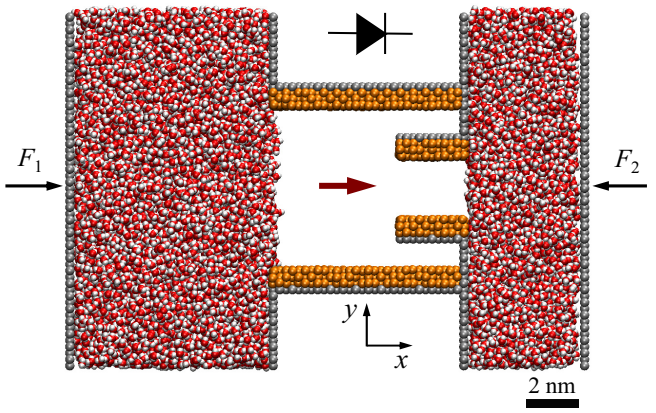

FIG. 1. Schematic of the fluidic diode system. Flows are only allowed in the forward direction (left to right) in certain pressure drop ranges.

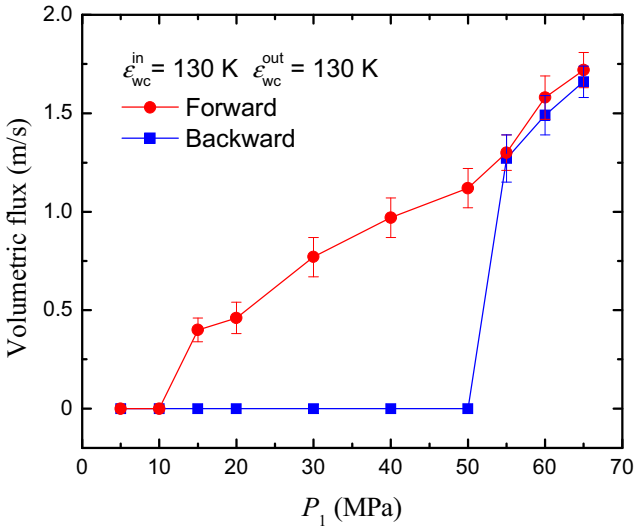

FIG. 2. Volumetric flux as a function of the driving pressure P_1 in the forward and backward directions ($\varepsilon_{wc}^{in} = \varepsilon_{wc}^{out} = 130$ K). P_1 varies from 5 to 65 MPa, and the downstream pressure P_2 is maintained at 2 MPa.

respectively. The heights of the inner and the outer channels in the y direction are 2 and 5 nm, respectively. The lengths of them in the x direction are 2 and 6 nm. The initial lengths of the left and right reservoirs in the x direction are 6.5 and 3.5 nm, respectively. The channel walls are constructed by truncating a rectangular portion from a face-centered cubic structure with a lattice constant equal to 4.086 Å. The outmost layers of the inner and outer channels are fixed to maintain a stable system, whereas the other layers (orange atoms) are free to vibrate to account for the flexibility of the walls. Initially, the reservoirs are filled with 11 500 water molecules, and the pressures of the reservoirs are controlled by applying an external force on the left and right rigid walls of the reservoirs as shown in Fig. 1.

The interactions among water molecules are described by the extended simple point charge potential. In this model, a water molecule contains an oxygen and two hydrogen atoms, all of which are charged. The interaction between a pair of water molecules includes both Coulombic and van der Waals forces [29,30]. The tight-binding potential, well accepted for transition metals, is used to model the channel walls, and the parameters for Ag are used [31,32]. The water-channel interaction is calculated by the Lennard-Jones (LJ) potential $U(r) = 4\varepsilon_{wc}[(\sigma_{wc}/r)^{12} - (\sigma_{wc}/r)^6]$, where ε_{wc} and σ_{wc} are the binding energy and the collision diameter. $\sigma_{wc} = 2.85$ Å is used based on the Lorentz-Berthelot mixing rule using the self-interaction LJ parameters for oxygen and Ag given in Refs. [33,34]. The surface wettabilities of the inner and outer channels are tuned by changing the water-channel binding energies ε_{wc}^{in} and ε_{wc}^{out}. The cutoff distance for all the potentials is set to be 1.3 nm, and the equations of motion are integrated using Beeman's algorithm with time steps equal to 1 fs. The temperature of the reservoirs and channels is controlled at 300 K using a Berendsen thermostat [35]. Periodic boundary conditions are employed in the y and z directions for water in the reservoirs and in the z direction for the channels.

III. RESULTS AND DISCUSSION

We first study the case where both channels have the same surface energy and are hydrophobic. The water-channel binding energy for both channels is set as $\varepsilon_{wc}^{in} = \varepsilon_{wc}^{out} = 130$ K for which the water contact angle is 92° [29]. The pressure of the downstream reservoir P_2 is maintained at 2 MPa, whereas the pressure of the upstream reservoir P_1 is varied from 5 to 65 MPa. Figure 2 shows the volumetric flux as a function of the driving pressure P_1 in the forward (left to right) and backward (right to left) directions. It is seen that there is a critical pressure, $P_F^* \sim 10$ and $P_B^* \sim 50$ MPa, for the forward and backward directions, below which water flows are not observed. P_F^* and P_B^* can be viewed as the activation pressures for turning on the water flows. When the driving pressure P_1 becomes higher than P_F^*, for $P_F^* < P_1 < P_B^*$, flows in the forward direction are allowed, but the flows in the backward direction are blocked. In this pressure range ($10 < P_1 < 50$ MPa), the nested nanochannel structure acts as a fluidic diode. As P_1 is further increased, flows in the backward direction are allowed, and the fluxes in both directions tend to be the same, which occurs for $P_1 > 55$ MPa and is similar to the breakdown of electronic diodes.

The anisotropic activation pressures P_F^* and P_B^* are the major parameters for the fluidic diode. Their values are determined by the distinct infiltration processes in the forward and backward directions. Before understanding P_F^* and P_B^*, it has to be noted that the pressure required to drive a fluid through a hydrophobic nanochannel consists of two parts. One is the capillary pressure given by the Young-Laplace equation $p = -2\gamma \cos\theta/H$, where γ and θ are the surface tension and contact angle of the fluid and H is the channel height. The other is the entrance barrier pressure $P_{\Delta E}$, which is caused by a potential energy barrier at the entrance of a hydrophobic nanochannel due to the water-channel molecular interactions [29]. For the proposed nanochannel structure, in the forward direction, the water transport from the left to the right reservoir contains two serial infiltration processes, i.e., the infiltrations into the outer and then inner channels, as illustrated in Figs. 3(a1) and 3(a2). The infiltration pressure for the inner channel is higher than that for the outer channel

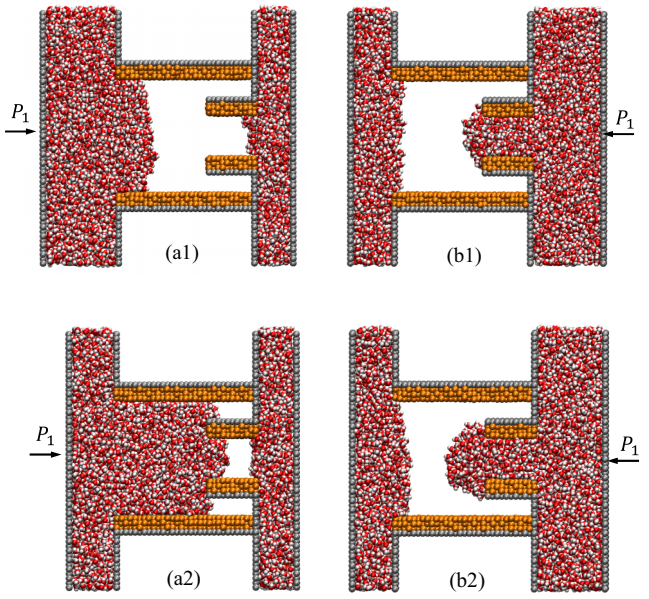

FIG. 3. Snapshots showing the meniscus at different stages in the forward [(a1) and (a2)] and backward [(b1) and (b2)] flows ($\varepsilon_{wc}^{in} = \varepsilon_{wc}^{out} = 130$ K).

and is obtained as 10 MPa using the method in Ref. [29], which is P_F^*. In the backward direction, the flow has to infiltrate into the inner channel first, which requires 10 MPa for the pressure of the right reservoir. However, when the water molecules move to the left end of the inner channel, the surface tension of the convex meniscus will stop the water flow if the upstream pressure is not further increased as shown in Fig. 3(b1). To overcome the resistance caused by the surface tension, the pressure of the right reservoir has to be higher than that predicted by the Young-Laplace equation $p = -2\gamma \cos\theta/H$, where θ is the largest contact angle for the meniscus as it evolves when the upstream pressure is gradually increased. For the case in Fig. 2, the largest contact angle is $138.3^\circ \pm 2.5^\circ$, which is obtained by fitting the density distribution of water with the isopycnic line of density equal to 300 kg m^3 [29,36] as illustrated in Figs. 3(b2) and 4(a). If water surface tension $\gamma = 71.6$ mN/m is used, the pressure needed to drive water molecules through the inner channel is predicted to be 53.5 MPa, which is the activation pressure P_B^* in the backward direction. Therefore, for the nested nanochannel system, P_F^* is determined by the infiltration pressure of the inner hydrophobic channel, whereas P_B^* is governed by the capillary pressure for the inner channel. If the upstream pressure is higher than P_B^*, both the infiltration and the capillary pressures become unimportant, and the flux in both directions tends to be the same. This is similar to the breakdown of electronic diodes. It is noted that the outer channel also plays an important role, especially in the backward direction. Its size has to be small, or the surface has to be sufficiently hydrophobic to make sure that water in the left reservoir does not infiltrate into the outer channel. Otherwise, the capillary effect at the outlet of the inner channel for backward flows will not take place, and the flows in both directions will be controlled by the infiltration pressure of the inner channel. In this case, flow rectifications will not be observed.

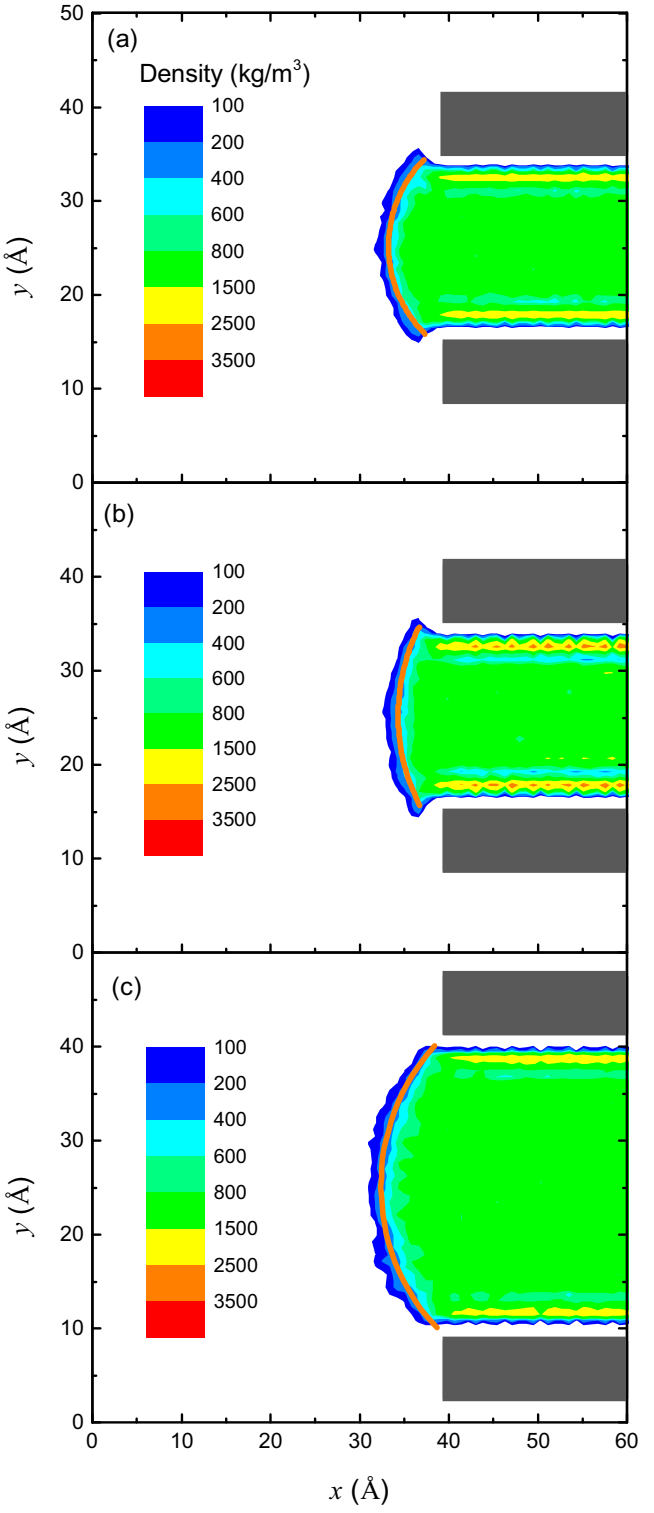

FIG. 4. Density contour of water in the inner channel for (a) $\varepsilon_{wc}^{in} = 130$ K and $H = 2$ nm, (b) $\varepsilon_{wc}^{in} = 200$ K and $H = 2$ nm, and (c) $\varepsilon_{wc}^{in} = 130$ K and $H = 3$ nm. The contact angle of water is determined by a series of isopycnic lines. The solid lines are isopycnic lines of density equal to 300 kg m^3.

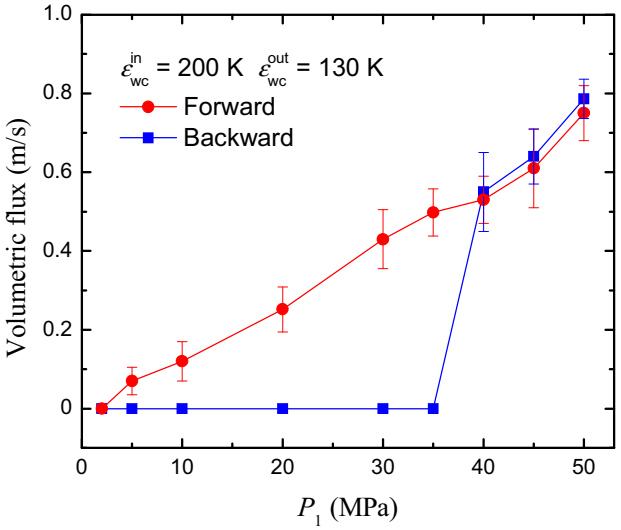

FIG. 5. Volumetric flux versus the driving pressure as the inner channel becomes hydrophilic ($\varepsilon_{wc}^{in} = 200$ K, $\varepsilon_{wc}^{out} = 130$ K). P_1 varies from 2 to 50 MPa, and P_2 is 2 MPa.

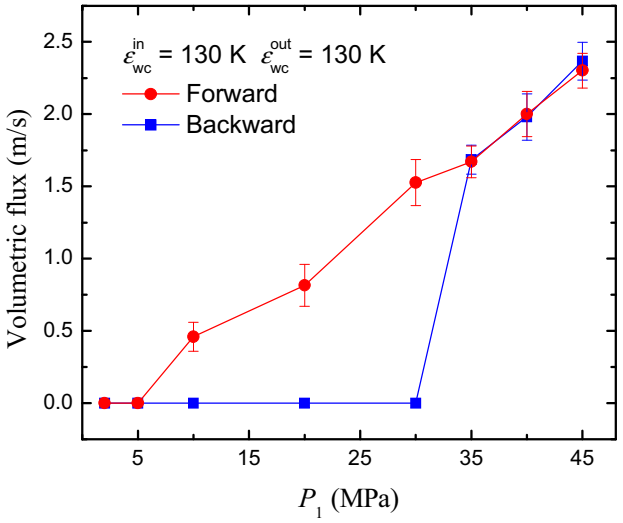

FIG. 6. Volumetric flux versus the driving pressure as the height of the inner channel is increased to 3 nm ($\varepsilon_{wc}^{in} = \varepsilon_{wc}^{out} = 130$ K). P_1 varies from 2 to 45 MPa, and P_2 is 2 MPa.

Since the activation pressures P_F^* and P_B^* are mainly determined by the inner channel, their values can be varied by changing the size and surface energy of the inner channel. If the inner channel is tuned to be hydrophilic, water infiltration into it will be automatic, which will lead to zero infiltration pressure, and the activation pressure in the forward direction P_F^* will be the infiltration pressure of the outer channel. Figure 5 depicts the flux in the nested channels when the inner channel surface energy is increased and the water-channel binding energy $\varepsilon_{wc}^{in} = 200$ K for which the water contact angle is 60°. It is seen that water flows are accepted in the forward direction when the upstream pressure is higher than 2 MPa, which corresponds to the infiltration pressure of the outer channel [29]. The activation pressure in the backward direction P_B^* is also reduced to 35 MPa because the largest contact angle during the release of water from the inner channel is lowered to $121.0° \pm 3.2°$ [Fig. 4(b)] for which the Young-Laplace equation predicts that the capillary pressure is 36.8 MPa. This is in good agreement with the MD result in Fig. 5.

The activation pressures P_F^* and P_B^* can also be adjusted by changing the inner channel height H. Figure 6 illustrates the flux in the nested channels when the height of the inner channel is increased to 3 nm. Compared to Fig. 2, the activation pressure in the forward direction P_F^* is reduced to 5 MPa, which is the infiltration pressure of the inner channel [29]. The activation pressure in the backward direction P_B^* is reduced to 30 MPa, mainly because of the increase in the channel height. In this case, the largest contact angle during the release of water from the inner channel is $136.8° \pm 2.8°$ [Fig. 4(c)], slightly lower than that of Fig. 2. The capillary pressure predicted by the Young-Laplace equation is 34.8 MPa, which is consistent with the MD result in Fig. 6.

It is worth mentioning that there might be optimal channel sizes and surface wettabilities for the fluidic diode and the geometry of the channel entrances could also be changed to improve the performance of the diode. These will be investigated in future work.

IV. CONCLUSIONS

To summarize, we have demonstrated a nested nanochannel structure to work as a fluidic diode for simple fluids in a wide range of pressure drops. The flow rectification effects are caused by direction dependent activation pressures due to different flow mechanisms in the forward and backward directions. The pressure drop range for the fluidic diode can be adjusted for practical applications by tuning the surface wettability or channel size.

ACKNOWLEDGMENTS

This work was supported by the Research Grants Council of the Hong Kong Special Administrative Region under Grant No. 16205714. J.M. was partially supported by a Postgraduate Scholarship through the Energy Program at HKUST.

[1] J. Bardeen and W. H. Brattain, Phys. Rev. **74**, 230 (1948).
[2] S. M. Sze and K. K. Ng, *Physics of Semiconductor Devices*, 3rd ed. (Wiley, Hoboken, NJ, 2007).
[3] B. Li, L. Wang, and G. Casati, Phys. Rev. Lett. **93**, 184301 (2004).
[4] L. Wang and B. Li, Phys. Rev. Lett. **101**, 267203 (2008).
[5] L. Wang and B. Li, Phys. Rev. Lett. **99**, 177208 (2007).
[6] C. W. Chang, D. Okawa, A. Majumdar, and A. Zettl, Science **314**, 1121 (2006).
[7] J. B. Boreyko, Y. Zhao, and C. H. Chen, Appl. Phys. Lett. **99**, 234105 (2011).

[8] B. Liang, X. S. Guo, J. Tu, D. Zhang, and J. C. Cheng, Nat. Mater. **9**, 989 (2010).
[9] B. Liang, B. Yuan, and J. C. Cheng, Phys. Rev. Lett. **103**, 104301 (2009).
[10] L. Li, J. Mo, and Z. Li, Phys. Rev. Lett. **115**, 134503 (2015).
[11] K. W. Oh and C. H. Ahn, J. Micromech. Microeng. **16**, R13 (2006).
[12] M. A. Unger, H. P. Chou, T. Thorsen, A. Scherer, and S. R. Quake, Science **288**, 113 (2000).
[13] A. W. Martinez, S. T. Phillips, Z. Nie, C. M. Cheng, E. Carrilho, B. J. Wiley, and G. M. Whitesides, Lab Chip **10**, 2499 (2010).
[14] T. Thorsen, S. J. Maerkl, and S. R. Quake, Science **298**, 580 (2002).
[15] J. Melin and S. R. Quake, Annu. Rev. Biophys. Biomol. Struct. **36**, 213 (2007).
[16] A. Groisman, M. Enzelberger, and S. R. Quake, Science **300**, 955 (2003).
[17] E. Delamarche, D. Juncker, and H. Schmid, Adv. Mater. **17**, 2911 (2005).
[18] J. W. Hong and S. R. Quake, Nat. Biotechnol. **21**, 1179 (2003).
[19] C. L. Hansen, E. Skordalakes, J. M. Berger, and S. R. Quake, Proc. Natl. Acad. Sci. USA **99**, 16531 (2002).
[20] N. Tesla, U.S. Patent No. 1,329,559 (3 Feb. 1920).
[21] A. Olsson, G. Stemme, and E. Stemme, Sens. Actuators, A **57**, 137 (1996).
[22] E. Stemme and G. Stemme, Sens. Actuators, A **39**, 159 (1993).
[23] A. Olsson, G. Stemme, and E. Stemme, Sens. Actuators, A **47**, 549 (1995).
[24] M. Nabavi, Microfluid. Nanofluid. **7**, 599 (2009).
[25] A. Groisman and S. R. Quake, Phys. Rev. Lett. **92**, 094501 (2004).
[26] P. C. Sousa, F. T. Pinho, M. S. N. Oliveira, and M. A. Alves, J. Non-Newtonian Fluid Mech. **165**, 652 (2010).
[27] H. Chen, J. Cogswell, C. Anagnostopoulos, and M. Faghri, Lab Chip **12**, 2909 (2012).
[28] J. E. Mates, T. M. Schutzius, J. Qin, D. E. Waldroup, and C. M. Megaridis, ACS Appl. Mater. Interfaces **6**, 12837 (2014).
[29] J. Mo, L. Li, J. Zhou, D. Xu, B. Huang, and Z. Li, Phys. Rev. E **91**, 033022 (2015).
[30] H. J. C. Berendsen, J. R. Grigera, and T. P. Straatsma, J. Phys. Chem. **91**, 6269 (1987).
[31] F. Cleri and V. Rosato, Phys. Rev. B **48**, 22 (1993).
[32] Z. Li and H. Wang, Phys. Rev. Lett. **95**, 014502 (2005).
[33] S. Chowdhuri and A. Chandra, J. Chem. Phys. **115**, 3732 (2001).
[34] Z. Li, Phys. Rev. E **79**, 026312 (2009).
[35] M. Allen and D. Tildesley, *Computer Simulation of Liquids* (Oxford University Press, New York, 1987).
[36] M. J. P. Nijmeijer, C. Bruin, A. F. Bakker, and J. M. J. Van Leeuwen, Physica A **160**, 166 (1989).